Accepted Manuscript

Formation of needle-like and honeycomb-like magnesium oxide/hydroxide structures by electrodeposition from magnesium nitrate melts

Vesna S. Cvetković, Nataša M. Vukićević, Nebojša D. Nikolić, Goran Branković, Tanja S. Barudžija, Jovan N. Jovićević

PII: S0013-4686(18)30425-0

DOI: 10.1016/j.electacta.2018.02.121

Reference: EA 31316

To appear in: *Electrochimica Acta*

Received Date: 15 December 2017

Revised Date: 22 February 2018

Accepted Date: 23 February 2018

Please cite this article as: V.S. Cvetković, N.M. Vukićević, N.D. Nikolić, G. Branković, T.S. Barudžija, J.N. Jovićević, Formation of needle-like and honeycomb-like magnesium oxide/hydroxide structures by electrodeposition from magnesium nitrate melts, *Electrochimica Acta* (2018), doi: 10.1016/j.electacta.2018.02.121.

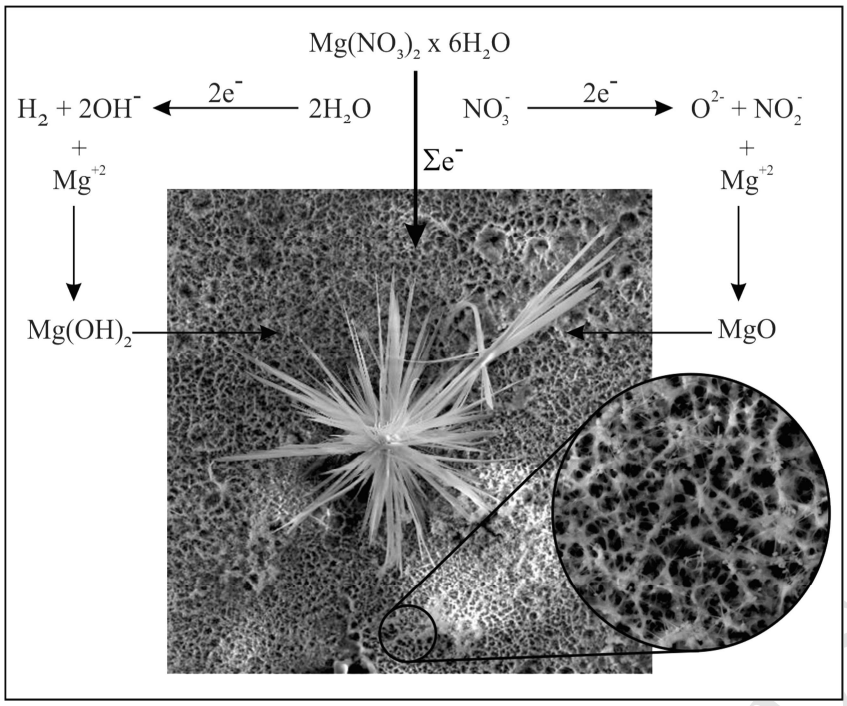

Formation of needle-like and honeycomb-like magnesium oxide/hydroxide structures by electrodeposition from magnesium nitrate melts

Vesna S. Cvetković[1], Nataša M. Vukićević[1], Nebojša D. Nikolić[1,*], Goran Branković[2], Tanja S. Barudžija[3], Jovan N. Jovićević[1]

[1]ICTM – Department of Electrochemistry, University of Belgrade, Belgrade, Njegoševa 12, Serbia

[2]Institute for Multidisciplinary Research, University of Belgrade, Belgrade, Kneza Višeslava 1a, Serbia

[3]Institute for Nuclear Sciences Vinča, University of Belgrade, P.O.Box 522, 11001 Belgrade, Serbia

Abstract

The processes of electrochemical deposition of magnesium oxide/hydroxide on glassy carbon (GC) electrode from magnesium nitrate hexahydrate melt have been investigated. A novel procedure predicting a possibility of direct formation of magnesium oxide during electrodeposition from the nitrate melt used is reported. XRD analysis of the obtained deposits showed the formation of magnesium oxide along with magnesium hydroxide. The electrodeposition of magnesium oxide/hydroxide commences in magnesium underpotential (UPD) and continues through the magnesium overpotential (OPD) region. Network of individual or intertwined very thin needles as well as those grouped in flower-like aggregates or honeycomb-like structures were formed in both magnesium UPD and OPD regions. Formation of the long needles was explained through theories of mechanisms of dendrite

* Corresponding author: nnikolic@tmf.bg.ac.rs; tel/fax: +381 11 3370389 (Dr. N.D. Nikolić)

formation. Hydrogen evolution commences in the magnesium OPD region and increases with the applied overpotential. Holes observed in the deposit originated from the detached hydrogen bubbles. The number, shape and size of the hole strongly depended on both the applied cathodic potential and the hold time of electrodeposition. Magnesium oxides/hydroxides syntheses taking part simultaneously at various applied potentials are a result of reactions between magnesium cations and products of water and nitrate anions reduction processes. Chemical reactions responsible for direct formation of magnesium oxide observed are those of magnesium ions and oxygen ions, formed by nitrate reduction taking part in the close vicinity of the working electrode.

Keywords: electrodeposition; melt; magnesium oxide/hydroxide; honeycomb; needles.

1. Introduction

Nanocrystalline magnesium oxide (MgO) and magnesium hydroxide $Mg(OH)_2$, are attracting comprehensive attention in both fundamental and application areas, due to their specific magnetic, optical, thermal, mechanical and chemical properties, as well as absorption ability, high surface reaction activity, high catalytic activity, and unique crystal and electronic structure [1–7]. Magnesium oxide and magnesium hydroxide, as non-toxic and non-corrosive materials, have been increasingly used in catalysis, medicine, toxic waste remediation, for superconducting and space flight composite materials [1,2,4,5,8–15].

Nanoscale magnesium hydroxide $Mg(OH)_n$ and magnesium oxide (MgO) whiskers with large surface area in the forms suitable for application in various technologies have received noteworthy recognition [1,16]. As a sensitive and selective tool for analytical application and diagnostic research, nano-sized MgO material has been recently used in the development of several electrochemical biosensors based on one-dimensional magnesium

oxide nanoparticles of various morphologies [9,17,18]. Additionally, porous $Mg(OH)_2$/MgO material used as adsorbent for removal of toxic ions (especially Cd^{2+} and Pb^{2+}) proved to be more effective than any other equivalent due to its unique micro/nano structure [19]. Furthermore, $Mg(OH)_2$/MgO as a large-band-gap (e.g., 5.17 eV) semi-conducting material is often applied in the next-generation solar cells [19,20]. At the same time, $Mg(OH)_2$ nanomaterials found their way as components in medical and pharmaceutical products [21].

Due to the fact that the composition and surface morphology of the resulting Mg oxide/hydroxide-nano sized crystals play an important role in applications with various technologies, it is only to be expected that special significance is paid to their synthesis and processing parameters. Magnesium oxide/hydroxide nanoparticles with different morphological structures have been obtained via different synthesis methods such as chemical precipitation [1,22], flame spray pyrolysis [23], electrostatic spray deposition [24], pulse laser deposition [25,26], electrolysis of aqueous magnesium salt solutions [16,18], plasma chemical vapor deposition [27,28], and sol-gel method as the most common way to obtain the nanoparticles [1,12,17,29,30]. Each method has its own advantages in various aspects, however, large scale synthesis of pure magnesium oxide/hydroxide with nanoscale controlled morphology is limited [1].

Unlike the methods listed above, electrochemical deposition provides a very suitable way for the synthesis of desired nanostructured deposits, because shape and size of the nanostructures can be conveniently controlled by the choice of parameters and regimes of electrolysis [31,32]. The process of magnesium hydroxide electrodeposition and subsequent magnesium oxide formation has been investigated mostly from magnesium nitrate hexahydrate aqueous solutions and the same solution with ethanol (50%:50%) [4,5,16,33]. Other authors have reported magnesium hydroxide nanoparticles electrochemically synthesized from magnesium chloride hexahydrate aqueous solution [34,35]. The product

from all of these processes was magnesium hydroxide and additional thermal treatment was required to obtain magnesium oxide.

In this study, a novel approach to electrochemical synthesis of magnesium oxide/hydroxide meso - and nanostructures is presented. Unlike previous investigations based on formation of these structures from aqueous solutions of magnesium nitrate hexahydrate without [18] or with additives, like sodium acetate [5] or potassium nitrate [4], this approach is based on the electrodeposition from the melt made of the same magnesium salt. The electrolysis from the aqueous electrolytes produced mainly uniform porous platelet-like magnesium hydroxide structures. Although hydrogen evolution was one of the main cathodic reactions, no attention was paid to its influence on the morphology of electrodeposited structures. Works on magnesium electrodeposition from magnesium nitrate melts [36–40] indicated magnesium oxide formation possibly by reaction of magnesium ions with oxygen ions formed by nitrate reduction. This novel method will show that magnesium oxide can be synthesized directly by electrodeposition from nitrate melt, thus avoiding additional thermal transformation treatments of initially formed magnesium hydroxide into oxide. One of the aims of this study was also to examine the effect of hydrogen evolution on the morphology of structures formed on the working electrode.

2. Experimental

To study magnesium oxide/hydroxide deposition from magnesium nitrate melt linear sweep voltammetry (LSV), potentiodynamic polarization scan and chronoamperometry were applied in a three electrode electrochemical cell under argon atmosphere using EG&G PAR 273A Potentiostat/Galvanostat controlled by Power Suite software (Princeton Applied Research, USA). Magnesium oxide/hydroxide was electrodeposited onto a cylindrical glassy

carbon working electrode (GC, Alfa Aeser-Johnson Mathey. Co, USA) placed in the center of the cell, with surface area of 0.8 cm^2 exposed to contact with the melt. The counter electrode was a Mg (99.999%, Luoyang Magnesium Gurnee Metal Material Company. Ltd, Henan, China) rectangular shovel (surface area = 7.5 cm^2). The reference electrode was a 3 mm diameter magnesium (99.999 %) wire positioned at a close distance of about 0.3 cm from the surface of the working electrode. Prior to the experiments, the reference and counter electrodes were chemically cleaned and etched [38–40]. Analytical grade $Mg(NO_3)_2 \cdot 6H_2O$ (J.T. Baker, The Netherlands), was used as the electrolyte, and after being added to the cell, it was carefully heated under argon atmosphere to the temperature of 100 ^oC.

The reported working electrode potentials were measured relative to the equilibrium potential of magnesium reference electrode in the melt used under given conditions [40]. The voltammograms were recorded as a response to the working electrode potential being scanned from a starting potential, E_S (usually 50 to 100 mV more negative to the reversible potential of the GC working electrode) to a final chosen negative potential, E_f followed by the return scan. The sweep rates used were between 1 mVs^{-1} and 50 mVs^{-1}.

Potentiostatic deposition process was carried out by changing the working electrode potential from an initial potential, E_i (50 to 100 mV more negative to the working electrode potential in the given melt) to a final potential, E_f (in magnesium UPD region at 700 mV, 5 mV vs. Mg and in magnesium OPD region at –200 mV, –1000 mV vs. Mg). The E_f potential was held constant for 30 or 120 minutes, at T= 100 °C, whereupon the working electrode was retrieved from the cell under potential in order to preserve deposited material.

The deposit obtained on the working electrode was washed with plenty of absolute ethanol (Zorka-Pharma, Šabac, Serbia) and dried in a desiccator furnished with silica gel. The morphology was studied using Scanning electron microscope – TESCAN Digital Microscope; model VEGA3, Brno, Czech Republic). For further characterization of structural

properties, the deposits were subjected to X-ray diffraction (Enraf-Nonius powder diffractometer, Delft, The Netherlands).

3. Results

3.1. **Electrochemical measurements**

Typical voltammograms recorded with a GC working electrode in magnesium nitrate melt used are shown in Fig. 1. In the potential range explored (from 1.400 V vs. Mg to –1.000 V vs. Mg) three broad reduction peaks were indicated and no anodic counterparts observed. Such broad peak shapes typically reflect processes that start successively one after the other at potentials whose values are close and proceed further simultaneously, thus making the recorded current at each potential the sum of rates of all the processes taking part at that particular potential. The absence of anodic counterparts to reduction peaks was a subject of discussion in a number of works [4,5,18,36–42]. This phenomenon was attributed to formation of the MgO and $Mg(OH)_2$ deposits during potential change into negative direction which do not dissolve when the potential is returned to the starting positive value. Results obtained by very slow potentiodynamic polarization of the working electrode under the same conditions are presented in Fig. 2, and they support the findings seen in generated voltammograms. While there were three evident current increases when electrode potential was changed toward negative values, there was a steady current decrease when potential was turned back toward positive values. Positions of the current density maxima on the potential axis were very close to those shown in voltammograms obtained under the same conditions. These values were guidelines for the chronoamperometry experiments that are shown in Fig. 3. Results of those experiments show current which, after a substantial initial value, fades

away into relatively small but permanent current which provides material for deposit formation.

3.2. **XRD analysis**

An XRD diagram of the deposit obtained is shown in Fig.4. This analysis identifies magnesium oxides and magnesium hydroxides as substances synthetized under cathodic potentiostatic regime. The recorded 2θ peak at 18.7°, according to some authors, reflects crystalline Mg(O,OH) deposit [20]. However, this 2θ value together with several other stronger diffraction peaks recorded (at 32.8°, 51.05°, 68.2° and 72.1°) could also be ascribed to hexagonal $Mg(OH)_2$ [JCPDS No. 01-083-0114]. The 2θ peak recorded at 29.2° belongs to face-centered cubic MgO [JCPDS No. 00-030-0794] and broader peaks at around 38°and 59° can be ascribed to both MgO and $Mg(OH)_2$ [JCPDS No. 00-030-0794, JCPDS No. 01-083-0114]. The peak at 2θ value of 43.05° belongs to MgO Periclase [JCPDS No. 01-075-1525], and that at 62.59° can be attributed both to MgO [JCPDS No. 01-075-1525] and to $Mg(OH)_2$ [JCPDS No. 01-083-0114]. There were no additional peaks in the XRD pattern recorded, which indicates that the MgO/$Mg(OH)_2$ particles produced by the electrochemical deposition method were relatively pure. However, it should be emphasized that the peaks recorded at 2θ values 29.2° and 43.05° are characteristic only to MgO.

3.3. **SEM results**

As previously noted, the electrodeposition process commences in the magnesium underpotential (UPD) region. Typical surface morphologies obtained at potentials of 700 mV and 5 mV vs. Mg with an electrodeposition time of 30 min are shown in Fig. 5. In both cases,

a network of intertwined thin needles, often referred as whiskers [43–45] were formed. At the potential of 700 mV vs. Mg, individual intertwined groups of needles were formed at the GC (Fig. 5a–c), while the whole GC electrode surface was covered by them at a potential of 5 mV vs. Mg (Fig. 5d and e).

A somewhat different situation is observed in the magnesium overpotential deposition (OPD) region. Typical surface morphologies obtained at different cathodic potentials and electrodeposition times are shown in Figs. 6–8. There are very thin needles, already observed in the UPD region, and holes in the deposit made by hydrogen evolution reaction.

Figure 6 shows the deposits obtained at a cathodic potential of –200 mV vs. Mg with an electrodeposition time of 30 min. The individual hole formed from the detached hydrogen bubble and a very thin needles oriented in all directions were formed by the electrodeposition at this potential (Fig. 6a). Analysis of the hole at a higher magnification (Fig. 6b) showed that its average diameter was about 150 μm. On the other hand, the very thin needles were grouped in flower-like forms like the one shown in Fig. 6c. The length of the formed needles was up to about 160 μm (Fig. 6c), while their diameter was smaller than 2 μm (Fig. 6d). Aside from the holes and the flower-like forms, careful analysis of the electrode surface (see the part in the circle in Fig. 6a) revealed the existence of very porous structure between them (Fig. 6e and f). The electrode surface between individual holes and the flower-like forms consisted of numerous relatively small holes and the thin needles formed around them. The average size of these holes was smaller than 4 μm (Fig. 6e and f). This very porous structure showing high uniformity represents the typical honeycomb-like structure [46] constructed from holes formed by the detached hydrogen bubbles and very thin needles around them. The number of holes formed from the detached hydrogen bubbles was estimated to be approximately 50000 holes per mm^2 electrode surface. Figure 7 shows morphologies of the deposit obtained at a potential of –200 mV vs. Mg with a time of electrodeposition of 2 h.

Matching the expectation, holes formed from the detached hydrogen bubbles and the thin needles remain the main morphological forms obtained at this potential (Fig. 7a). The size of holes and the length of needles increased with increased time of electrodeposition. That can be estimated from Fig. 7b, which shows a typical hole formed from the detached hydrogen bubble, and from Fig. 7c which shows a network of intertwined needles. The average size of holes obtained with electrodeposition time of 2 h was about 240 μm (Fig. 7b). As a result, hole size increase of about 60 % was observed with fourfold increase of electrodeposition time. Simultaneously, the length of needle-like forms was up to 400 μm (Fig. 7c), which represents an increase of more than 2.5 times compared to those obtained with an electrodeposition time of 30 min. The bottom of the holes was constructed from thin needles (see insert in Fig. 7b). It should be noted that the flower-like structure observed with the electrodeposition time of 30 min (Fig. 6c) was lost with the prolonged electrodeposition process. The very porous structure (the honeycomb-like one) observed with an electrodeposition time of 30 min (Fig. 6e) also suffered strong transformation with increasing electrodeposition time. Morphologies of the deposits corresponding to this part of the electrode surface but obtained after 2 h electrodeposition are shown in Fig. 7d–f. The average hole size in the honeycomb-like structure obtained after 2 h electrodeposition was about 20 μm, while the estimated number of the formed holes was about 1390 holes per mm^2 electrode surface. The intertwined very thin needle-like forms making the dense network were formed around the holes formed from the detached hydrogen bubbles (Fig. 7e). The diameter of the formed filaments or needles was less than 200 nm (Fig. 7f). The specific surface area of the honeycomb-like structures is determined by the number and size of holes, as well as by wall width among them [47,48]. The dramatic decrease in the number of the formed holes, and hence, the strong change of the specific surface area of this electrode type with increasing the electrodeposition time can be ascribed to a coalescence of neighboring hydrogen bubbles, but

also by the fact that the fast growth of needles in all directions can limit the growth of some bubbles so that they remain captured under fast-growing needles. The similar effect on the specific surface area of the honeycomb-like electrodes has been already observed in the case of copper electrodeposition from the aqueous electrolyte in the hydrogen co-deposition range [49].

Holes formed from the detached hydrogen bubbles and network of the intertwined thin needles (the honeycomb-like structure) are also formed at cathodic potentials higher than –200 mV vs. Mg. Figure 8 shows the deposits obtained at a potential of –1000 V vs. Mg with an electrodeposition time of 2 h. From Fig. 8, it can be seen that the diameter of holes was approximately 40 μm (Fig. 8b), which is six times smaller than those formed at –200 mV vs. Mg. The length of some of needles was up to 150 μm. All used potentials, the times of electrodeposition and the obtained morphologies of $MgO/Mg(OH)_2$ structures are summarized in Table 1.

4. Discussion

Mechanisms of $MgO/Mg(OH)_2$ formation on several electrodes by electrodeposition from aqueous, mostly nitrate solutions have been proposed in literature [4,5,16,18,33]. Those processes include heating of the obtained magnesium $MgO/Mg(OH)_2$ deposit at temperatures exceeding 350°C in order to produce magnesium oxide. Regrettably, this thermal treatment substantially changes appearance, morphology and crystal structure of the MgO crystallites obtained from initially well-developed very small and nano sized $MgO/Mg(OH)_2$ particles [33].

Possible characteristic of the processes provoking LSV reduction peaks in this work, have been proposed earlier, (Eq. (1) to (13)) [36–40]. To be used in this discussion, the

potentials given in some of those works [36,37] and attributed to the processes (1) to (9) should be corrected for the difference between the reversible potentials of Na, K and Li in their nitrate melts and Mg in used $Mg(NO_3)_2 \cdot 6H_2O$ melt. However, with enough certainty, one can suppose that the sequence with respect to the magnesium reversible potential and the differences between the potentials of the processes presented in Eq. (1) to (9) would be preserved in magnesium nitrate melt used as well.

1. $2NO_3^- + 6H_2O + 10e^- \leftrightarrow N_2 + 12OH^-$

2. $NO_3^- + H_2O + 2e^- \leftrightarrow NO_2^- + 2OH^-$

3. $NO_3^- + 5e^- \leftrightarrow \frac{1}{2}N_2 + 3O^{2-}$

4. $NO_3^- + 2e^- \leftrightarrow NO_2^- + O^{2-}$

5. $2NO_3^- + 2e^- \leftrightarrow 2NO_2^- + O_2^{2-}$

6. $2NO_3^- + 8e^- \leftrightarrow N_2O + 5O^{2-}$

7. $NO_3^- + 3e^- \leftrightarrow NO + 2O^{2-}$

8. $2NO_3^- + e^- \leftrightarrow 2NO_2^- + O^{2-}$

9. $NO_3^- + e^- \leftrightarrow NO_2 + O^{2-}$

For the melt used in this work additional reaction should be taken into account [18]:

10. $2H_2O + 2e^- \rightarrow 2OH^- + H_2$

not omitting reactions leading to $Mg(OH)_2$ and MgO formation:

11. $Mg^{2+} \cdot 2H_2O + 2e^- \rightarrow Mg(OH)_2 + H_2$

12. $Mg^{2+} + 2OH^- \rightarrow Mg(OH)_2$

13. $Mg^{2+} + O^{2-} \rightarrow MgO$

Having the preceding in mind, it can be assumed that voltammetry peak I (Fig. 1), recorded at potentials between ≈ 800 and ≈ 0 mV vs. Mg, reflects the most anodic group of anion reduction processes (mainly reactions 1 and 2); peak II, the second group of anion reduction processes (reactions 3–7) including some traces of water (reaction 10) and Mg^{2+} ions being reduced at potentials between 0 mV up to –350 mV vs. Mg; and finally, peak III at potentials more negative than –350 mV vs. Mg where more pronounced hydrogen evolution (reaction 10) joints a number of intensive nitrate anions reduction processes (processes 8 and 9). Magnesium oxide and hydroxide synthesis from the products of the reactions sited proceeds at the electrode surface within the whole potential range applied (reactions 11–13). It appears that possible individual and rare grains of electrodeposited magnesium become quickly covered with oxide or hydroxide.

The currents recorded obviously do not reflect Mg^{2+} reduction alone, in fact they predominantly reflect reactions described by Eqs. (1–13). This suggests that initial deposits were formed quickly and their precipitation on the electrode surface can cause pseudo-passivation [5,18,33,36]. However, H_2 bubbles produced on the electrode substrate and their detachment, sometimes provided a fresh area for the electrochemical reactions, reflected in a sudden current rise during longer deposition time intervals of chronoamperometric experiments, Fig. 3b.

As expected, the morphology of the deposits formed is dependent on the potential applied. The results obtained suggest that every amount of reactive magnesium on the electrode surface in the presence of O^{2-} and OH^- anions very quickly becomes a MgO or $Mg(OH)_2$ deposit. Therefore, the surface of the working electrode becomes partially covered with MgO even in the first most anodic part of linear change of the potential. Fast and unavoidable formation of insoluble MgO from used nitrate melts explains the lack of anodic current peaks on the voltammograms recorded.

As already mention in Section 3.3, two types of surface morphology are formed during electrodeposition from the nitrate melt: a) the very thin needles or filaments, and b) the holes originating from the detached hydrogen bubbles. Formation of the needle-like forms commences in the magnesium UPD, and continues throughout the examined magnesium OPD region. Dependending on the applied potential, these needles are grouped into either the flower-like forms or the network of intertwined thin needles. Formation of these structures clearly indicates strong diffusion control of the deposition process through the whole range of the examined potentials.

Formation of very long needles can be explained by theories about dendrite deposits formation by electrodeposition processes proposed by Diggle et al. [50] and Popov et al. [32,51,52]. According to these theories, the origin of needle-like forms, as well as the other types of dendrites is of surface protrusions formed in the initial stage of electrodeposition [32,51,52]. These surface protrusions are deeply buried in the diffusion layer of the macroelectrode, which is characterized by a steady linear diffusion to the flat portion of the electrode surface. The spherical diffusion layers are formed around the tips of such protrusions, and the current densities at them are greater than the corresponding linear diffusion current density. These local current densities caused by formation of the spherical diffusion fields correspond to the activation controlled electrodeposition [31,50,51]. Hence, it follows that electrodeposition processes at the tips of protrusions occur under activation control relative to the surrounding solution, and under diffusion control relative to the bulk solution. The current density at the tip of each of the formed protrusions corresponding to the activation controlled electrodeposition is simultaneously maximum rate of growth, that is confirmed by a considerable increase of the length of needles with time of electrodeposition (the maximum length of needles increased from 160 to 400 μm with prolonging the deposition time from 0.5 to 2 h). The growth of the needles in all directions confirms the

strong diffusion control of electrodeposition. Of course, considering mechanism of formation of the needle-like forms, it should not exclude the possibility that precipitation reactions like (12) and (13) affect the final shape of the needles. Such possibile influence on surface morphology has been already observed by Schiavi et al. [53] in the case of cobalt electrodeposition.

In the magnesium OPD region, hydrogen evolution reaction as a competitive to the others commences together with Mg electrodeposition process. Analysis of Figures 6–8 indicates that intensification of hydrogen evolution occurs with the increase in the cathodic potential value. Individual holes, referred to as dish-like ones [54], are formed at a potential of –200 mV vs. Mg (Fig. 6a and b). As is already known, formation of this type of holes, occurs with a small amount of evolved hydrogen. As expected, the diameter of the holes increases with time of the electrodeposition (Figs. 6a and b, 7a and b). As a result of intensification of hydrogen evolution, the number of holes increased, while their diameter decreased with the increase of the cathodic potential. Hence, it is clear that the phenomena established during metal electrodeposition from aqueous electrolytes in the hydrogen co-deposition range seen in works [32,49,55,56] are consistent with observations seen during MgO/$Mg(OH)_2$ electrodeposition processes from the nitrate melt.

Anyway, unlike electrodeposition from the aqueous nitrate electrolytes where only $Mg(OH)_2$ was formed, electrodeposition from the nitrate melt led to formation of MgO as well. The possibility that MgO can be obtained directly by the electrodeposition process from the melt represents a good basis for further research. The aim should be to increase MgO yield as much as possible, thus avoiding additional thermal treatment of initially formed $Mg(OH)_2$.

4. Conclusions

A novel method based on the electrolysis of the molten magnesium nitrate hexahydrate enabling simultaneous formation of magnesium oxide and hydroxide has been proposed. For the first time a direct formation of magnesium oxide during electrodeposition from the nitrate melt used is reported. The direct formation of magnesium oxide described here includes reactions of magnesium ions with oxygen ions, which are result of nitrate ions reduction, very close to the cathode surface. Chemistry of magnesium hydroxide formation from magnesium nitrate hexahydrate followed earlier proposed reactions between magnesium and hydroxide ions in water electrolytes. Main morphological forms of the deposits obtained by the electrochemical deposition processes were: very thin needle-like forms and holes formed from the detached hydrogen bubbles. In the dependence of the applied cathodic potentials, the thin needles are either intertwined into an elaborate network or they make flower-like aggregates. The thin needle-like forms are formed in both magnesium UPD and OPD regions, and their formation and growth are a diffusion-controlled process. The holes as a result of hydrogen evolution, occur only in the OPD region. The number of holes increased, while their diameter decreased with the increasing cathodic potential. The size of holes increased with increased time of the electrodeposition.

Acknowledgments: This work was supported by the Ministry of Education, Science and Technological Development of the Republic of Serbia (Grant No. 172046 and Grant No. 172060).

371 REFERENCES

372 [1] N.M. Julkapli, S. Bagheri, Magnesium oxide as a heterogeneous catalyst support, Rev.
373 Inorg. Chem. 36 (2016) 1–41. doi:10.1515/revic-2015-0010.
374 [2] Y. Ding, G. Zhang, H. Wu, B. Hai, L. Wang, Y. Qian, Nanoscale Magnesium
375 Hydroxide and Magnesium Oxide Powders: Control over Size, Shape, and Structure
376 via Hydrothermal Synthesis, Chem. Mater. 13 (2001) 435–440.
377 doi:10.1021/cm000607e.
378 [3] S. Utamapanya, K.J. Klabunde, J.R. Schlup, Nanoscale metal oxide particles/clusters
379 as chemical reagents. Synthesis and properties of ultrahigh surface area magnesium
380 hydroxide and magnesium oxide, Chem. Mater. 3 (1991) 175–181.
381 doi:10.1021/cm00013a036.
382 [4] G. Zou, R. Liu, W. Chen, Highly textural lamellar mesostructured magnesium
383 hydroxide via a cathodic electrodeposition process, Mater. Lett. 61 (2007) 1990–1993.
384 doi:10.1016/j.matlet.2006.07.172.
385 [5] G. Zou, W. Chen, R. Liu, Z. Xu, Morphology-tunable synthesis and characterizations
386 of $Mg(OH)_2$ films via a cathodic electrochemical process, Mater. Chem. Phys. 107
387 (2008) 85–90. doi:10.1016/j.matchemphys.2007.06.046.
388 [6] K.D. Bhatte, D.N. Sawant, K.M. Deshmukh, B.M. Bhanage, R. Rusdi, N. Kamarudin,
389 M. Llanos, E. Lopez-Salinas, Additive free microwave assisted synthesis of
390 nanocrystalline $Mg(OH)_2$ and MgO, Particuology. 10 (2012) 384–387.
391 doi:10.1016/j.partic.2011.05.004.
392 [7] J.C. Yu, A. Xu, L. Zhang, R. Song, L. Wu, Synthesis and Characterization of Porous
393 Magnesium Hydroxide and Oxide Nanoplates, J. Phys. Chem. B. 108 (2004) 64–70.
394 doi:10.1021/jp035340w.
395 [8] K.V. Rao, C.S. Sunandana, Structure and microstructure of combustion synthesized

MgO nanoparticles and nanocrystalline MgO thin films synthesized by solution growth route, J. Mater. Sci. 43 (2008) 146–154. doi:10.1007/s10853-007-2131-7.

[9] A. Umar, M.M. Rahman, Y.-B. Hahn, MgO polyhedral nanocages and nanocrystals based glucose biosensor, Electrochem. Commun. 11 (2009) 1353–1357. doi:10.1016/j.elecom.2009.04.033.

[10] Y. Jia, T. Luo, X.-Y. Yu, B. Sun, J.-H. Liu, X.-J. Huang, A facile template free solution approach for the synthesis of dypingite nanowires and subsequent decomposition to nanoporous MgO nanowires with excellent arsenate adsorption properties, RSC Adv. 3 (2013) 5430–5437. doi:10.1039/c3ra23340e.

[11] P. Jeevanandam, R.S. Mulukutla, Z. Yang, H. Kwen, K.J. Klabunde, Nanocrystals to nanorods: A precursor approach for the synthesis of magnesium hydroxide nanorods from magnesium oxychloride nanorods starting from nanocrystalline magnesium oxide, Chem. Mater. 19 (2007) 5395–5403. doi:10.1021/cm070666t.

[12] M. Mastuli, N. Kamarulzaman, M. Nawawi, A. Mahat, R. Rusdi, N. Kamarudin, Growth mechanisms of MgO nanocrystals via a sol-gel synthesis using different complexing agents, Nanoscale Res. Lett. 9 (2014) 134–143. doi:10.1186/1556-276X-9-134.

[13] X. Wang, D. Xue, Direct observation of the shape evolution of MgO whiskers in a solution system, Mater. Lett. 60 (2006) 3160–3164. doi:10.1016/j.matlet.2006.02.066.

[14] Y. Chen, J. Li, Y. Han, X. Yang, J. Dai, The effect of Mg vapor source on the formation of MgO whiskers and sheets, J. Cryst. Growth. 245 (2002) 163–170. doi:10.1016/S0022-0248(02)01690-1.

[15] M.R. Bindhu, M. Umadevi, M. Kavin Micheal, M.V. Arasu, N. Abdullah Al-Dhabi, Structural, morphological and optical properties of MgO nanoparticles for antibacterial applications, Mater. Lett. 166 (2016) 19–22. doi:10.1016/j.matlet.2015.12.020.

421 [16] M. Dinamani, P.V. Kamath, Electrosynthesis of $Mg(OH)_2$ Coatings on Stainless Steel
422 Substrates, J. Appl. Electrochem. 34 (2004) 899–902.
423 doi:10.1023/B:JACH.0000040437.81319.56.
424 [17] J. Ma, C.Z. Chen, D.G. Wang, J.H. Hu, Synthesis, characterization and in vitro
425 bioactivity of magnesium-doped sol-gel glass and glass-ceramics, Ceram. Int. 37
426 (2011) 1637–1644. doi:10.1016/j.ceramint.2011.01.043.
427 [18] C.-F. Li, W.-H. Ho, S.-K. Yen, Effects of Applied Voltage on Morphology and Crystal
428 Orientation of $Mg(OH)_2$ Coating on Pt by Electrochemical Synthesis, J. Electrochem.
429 Soc. 156 (2009) E29–E34. doi:10.1149/1.3032174.
430 [19] P.S. Das, A. Dey, A.K. Mandal, N. Dey, A.K. Mukhopadhyay, Synthesis of $Mg(OH)_2$
431 micro/nano flowers at room temperature, J. Adv. Ceram. 2 (2013) 173–179.
432 doi:10.1007/s40145-013-0058-9.
433 [20] C.-H. Huang, Y.-L. Jan, W.-C. Lee, Investigation of Mg(O,OH) Films Prepared by
434 Chemical Bath Deposition as Buffer Layers for $Cu(In,Ga)Se_2$ Solar Cells, J.
435 Electrochem. Soc. 158 (2011) H879–H888. doi:10.1149/1.3609047.
436 [21] C. Dong, J. Cairney, Q. Sun, O. Maddan, Lee, G. He, Y. Deng, Investigation of
437 $Mg(OH)_2$ nanoparticles as an antibacterial agent, J. Nanopart. Res. 12 (2010) 2101–
438 2109. doi:10.1007/s11051-009-9769-9.
439 [22] C. Henrist, J.P. Mathieu, C. Vogels, A. Rulmont, R. Cloots, Morphological study of
440 magnesium hydroxide nanoparticles precipitated in dilute aqueous solution, J. Cryst.
441 Growth. 249 (2003) 321–330. doi:10.1016/S0022-0248(02)02068-7.
442 [23] S. Demirci, B. Öztürk, S. Yildirim, F. Bakal, M. Erol, O. Sancakoğlu, R. Yigit, E.
443 Celik, T. Batar, Synthesis and comparison of the photocatalytic activities of flame
444 spray pyrolysis and sol–gel derived magnesium oxide nano-scale particles, Mater. Sci.
445 Semicond. Process. 34 (2015) 154–161. doi:10.1016/j.mssp.2015.02.029.

[24] S.G. Kim, H.C. Kook, J.H. Eun, H.J. Kim, C.S. Hwang, Effects of additives on properties of MgO thin films by electrostatic spray deposition, Thin Solid Films. 377–378 (2000) 694–698. doi:10.1016/S0040-6090(00)01283-9.

[25] T.J. Zhu, L. Lu, X.B. Zhao, Orientation of MgO thin films grown by pulsed laser deposition, Mater. Sci. Eng. B. 129 (2006) 96–99. doi:10.1016/j.mseb.2005.12.026.

[26] K. Nagashima, T. Yanagida, H. Tanaka, T. Kawai, Epitaxial growth of MgO nanowires by pulsed laser deposition, J. Appl. Phys. 101 (2007) 124304. doi:10.1063/1.2748625.

[27] Y.-W. Zhao, H. Suhr, Thin films of magnesium oxide prepared by plasma-enhanced chemical vapour deposition, Appl. Phys. A Solids Surfaces. 54 (1992) 451–454. doi:10.1007/BF00324170.

[28] K. Oumi, H. Matsumoto, K. Kashiwagi, Y. Murayama, MgO thin films for plasma display panel formed by plasma process, Surf. Coatings Technol. 169 (2003) 562–565. doi:10.1016/S0257-8972(03)00081-1.

[29] P. Tamilselvi, A. Yelilarasi, M. Hema, R. Anbarasan, Synthesis of hierarchical structured MgO by sol-gel method, Nano Bull. 2 (2013) 130106. doi:10.1234/NANO130106.

[30] R. Portillo, T. Lopez, R. Gomez, Magnesia Synthesis via Sol - Gel: Structure and Reactivity, Langmuir. 12 (1996) 40–44. doi:10.1021/la940694n.

[31] A.R. Despić, K.I. Popov, Transport controlled deposition and dissolution of metals, in: B.E. Conway, J.O.M. Bockris (Eds.), Mod. Asp. Electrochem., Plenum Press, New York, 1972: pp. 199–313.

[32] K.I.Popov, S.S.Djokić, N.D.Nikolić, V.D. Jović, Morphology of Electrochemically and Chemically Deposited Metals, Springer International Publishing, 2016.

[33] R. Hashaikeh, J.A. Szpunar, Electrolytic processing of MgO coatings, J. Phys. Conf.

Ser. 165 (2009) 12008. doi:10.1088/1742-6596/165/1/012008.

[34] Y. Matsumoto, T. Morikawa, H. Adachi, J. Hombo, A new preparation method of barium titanate perovskite film using electrochemical reduction, Mater. Research Bull. 27 (1992) 1319–1327. doi:10.1016/0025-5408(92)90097-J.

[35] G.H.A. Therese, P. V Kamath, Cathodic reduction of different metal salt solutions - Part I: Synthesis of metal hydroxides by electrogeneration of base, J. Appl. Electrochem. 28 (1998) 539–543. doi:10.1023/A:1003277430383.

[36] D.A. Tkalenko, Electrokhimiya Nitratnykh Rasplavov, Naukova Dumka, Kiev, Ukraine, 1983.

[37] D.A. Tkalenko, Makrokinetika Katodnykh Protsessov v Gidroksidnykh i Nitratnykh Rasplavakh, Naukova Dumka, Kiev, Ukraine, 1993.

[38] V.S. Cvetković, L.J. Bjelica, N.M. Vukićević, J.N. Jovićević, Alloy Formation by Mg Under-Potential Deposition on Al from Nitrate Melts, Chem. Ind. Chem. Eng. Q. 21 (2015) 527–536. doi:10.2298/CICEQ141205009C.

[39] V.S. Cvetković, J.N. Jovićević, L.J. Bjelica, Magnesium underpotential deposition from nitrate melts and alloy formation with platinum substrate, Kov. Mater. 54 (2016) 321–330. doi:10.4149/km_2016_5_1.

[40] V. Cvetković, N. Jovićević, J. Stevanović, M. Pavlović, N. Vukićević, Z. Stevanović, J. Jovićević, Magnesium–Gold Alloy Formation by Underpotential Deposition of Magnesium onto Gold from Nitrate Melts, Metals (Basel). 7 (2017) 95. doi:10.3390/met7030095.

[41] K. Bhatia, R.C. Sharma, H.C. Gaur, Conductivity of molten hydrated salts: $Mg(NO_3)_2 \cdot 6H_2O + NH_4NO_3$ system, Electrochim. Acta. 23 (1978) 1367–1369. doi:10.1016/0013-4686(78)80018-8.

[42] K.V. Ramana, R.C. Sharma, H.C. Gaur, Conductivity and viscosity of molten mixtures

of ferric nitrate nonahydrate with hydrates of calcium, cadmium, magnesium, and zinc nitrates, J. Chem. Eng. Data. 35 (1990) 293–297. doi:10.1021/je00061a020.

[43] Y. Chen, J. Li, Y. Han, X. Yang, J. Dai, Growth and characterization of dumbbell-shaped MgO nanowhiskers, Ceram. Int. 29 (2003) 663–666. doi:10.1016/S0272-8842(02)00214-6.

[44] Q. Wei, C.M. Lieber, Solution-Based Synthesis of Magnesium Oxide Nanorods, MRS Proc. 581 (1999) 3. doi:10.1557/PROC-581-3.

[45] Z. Wei, H. Qi, P. Ma, J. Bao, A new route to prepare magnesium oxide whisker, Inorg. Chem. Commun. 5 (2002) 147–149. doi:10.1016/S1387-7003(01)00367-7.

[46] N.D. Nikolić, K.I. Popov, Lj.J. Pavlović, M.G. Pavlović, The effect of hydrogen codeposition on the morphology of copper electrodeposits. I. The concept of effective overpotential, J. Electroanal. Chem. 588 (2006) 88–98. doi:10.1016/j.jelechem.2005.12.006.

[47] H.-C. Shin, M. Liu, Copper foam structures with highly porous nanostructured walls, Chem. Mater. 16 (2004) 5460–5464. doi:10.1021/cm048887b.

[48] N.D. Nikolić, G. Branković, Comparison of open porous copper structures obtained by the different current regimes of electrolysis, Mater. Lett. 70 (2012) 11–15. doi:10.1016/j.matlet.2011.11.081.

[49] N.D. Nikolić, K.I. Popov, Lj.J. Pavlović, M.G. Pavlović, Morphologies of copper deposits obtained by the electrodeposition at high overpotentials, Surf. Coat. Technol. 201 (2006) 560–566. doi:10.1016/j.surfcoat.2005.12.004.

[50] J.W. Diggle, A.R. Despic, J.O. Bockris, The Mechanism of the Dendritic Electrocrystallization of Zinc, J. Electrochem. Soc. 116 (1969) 1503–1514. doi:10.1149/1.2411588.

[51] K.I. Popov, N.D. Nikolić, General Theory of Disperse Metal Electrodeposits

Formation, in: S.S. Djokić (Ed.), Electrochemical Production of Metal Powders, Series: Mod. Asp. Electrochem., Springer International Publishing, 2012: pp. 1–62.

[52] K.I. Popov, N.V. Krstajić, M.I. Čekerevac, The mechanism of formation of coarse and disperse electrodeposits, in: R.E. White, B.E. Conway, J.O. Bockris (Eds.), Mod. Asp. Electrochem., Plenum Press, New York, 1996: pp. 261–312.

[53] P.G. Schiavi, P. Altimari, R. Zanoni, F. Pagnanelli, Morphology-controlled synthesis of cobalt nanostructures by facile electrodeposition: transition from hexagonal nanoplatelets to nanoflakes, Electrochim. Acta. 220 (2016) 405–416. doi:10.1016/j.electacta.2016.10.117.

[54] N.D. Nikolić, Lj.J. Pavlović, M.G. Pavlović, K.I. Popov, Formation of dish-like holes and a channel structure in electrodeposition of copper under hydrogen co-deposition, Electrochim. Acta. 52 (2007) 8096–8104. doi:10.1016/j.electacta.2007.07.008.

[55] N.D. Nikolić, K.I. Popov, Hydrogen Co-deposition Effects on the Structure of Electrodeposited Copper, in: S.S. Djokić (Ed.), Electrodeposition: Theory and Practice, Series: Mod. Asp. Electrochem., Springer-Verlag, 2010: pp. 1–70.

[56] S. Cherevko, X. Xing, C. Chung, Hydrogen template assisted electrodeposition of sub-micrometer wires composing honeycomb-like porous Pb films, Appl. Surf. Sci. 257 (2011) 8054–8061. doi:10.1016/j.apsusc.2011.04.098.

Figure captions:

Figure 1. Cyclic voltammograms on GC electrode obtained with scan rate 20 mVs^{-1} in magnesium nitrate melt at 100 °C: E_i = 1400 mV to E_f = (red line) –200 mV; (black line) –500 mV and (blue line) –1000 mV; Inset: Voltammogram with cathodic end potential in Mg UPD potential region.

Figure 2. Potentiodynamic polarization curves on GC electrode in magnesium nitrate melt at 100 °C, v = 1mV/s; (black line) E_i = 1500 mV → E_f = –1000 mV; (red line) E_i = –1000 mV → E_f =1300 mV.

Figure 3. a) and b) Current density – time transients on GC electrode, recorded at chosen cathodic end potentials during Mg deposition from magnesium nitrate melt at 100 °C; deposition time τ =2 hours.

Figure 4. X-ray diffraction patterns of electrochemically produced $MgO/Mg(OH)_2$ deposit on GC working electrode from magnesium nitrate melt at an overpotential of –200 mV at 100 °C, deposition time τ =2 hours.

Figure 5. $MgO/Mg(OH)_2$ deposits obtained in magnesium UPD region at various potentials: a)–c) 700 mV, and d) and e) 5 mV. In both cases, network of intertwined needles was formed.

Figure 6. $MgO/Mg(OH)_2$ deposits obtained in magnesium OPD region at a potential of –200 mV with electrodeposition time of 30 min: a) top view; b) a dish-like hole formed from detached hydrogen bubble; c) a flower-like aggregate constructed from very thin needles; d) a group of needles, and e) and f) honeycomb-like structure (surface area inside the circle in Fig. 6a).

Figure 7. $MgO/Mg(OH)_2$ deposits obtained in magnesium OPD region at a potential of –200 mV with electrodeposition time of 2 h: a) top view; b) a typical hole formed from a detached hydrogen bubble; c) network of intertwined needles; d)– f) honeycomb-like structure formed among large holes.

Figure 8. $MgO/Mg(OH)_2$ deposits obtained in magnesium OPD region at a potential of –1000 mV with electrodeposition time of 2 h: a) top view; b) the holes formed from detached hydrogen bubbles surrounded by very thin needles; c) needles formed around the holes, and d) network of intertwined very long needles.

Table 1: The values of cathodic potentials and times of electrodeposition used for formation $MgO/Mg(OH)_2$ structures and the corresponding electrodeposited surface morphologies.

No.	The potential / mV vs. Mg	The time of electrodeposition / min	Morphologies of electrodeposited $MgO/Mg(OH)_2$ structures
1.	700	30	– a network of intertwined needles
2.	5	30	– a network of intertwined needles
3.	– 200	30	– flower-like forms constructed from very thin needles, – dish-like hole, – the honeycomb-like structure
4.	– 200	120	– a network of intertwined needles, – individual holes, – the honeycomb-like structure
5.	– 1000	120	– the honeycomb-like structure

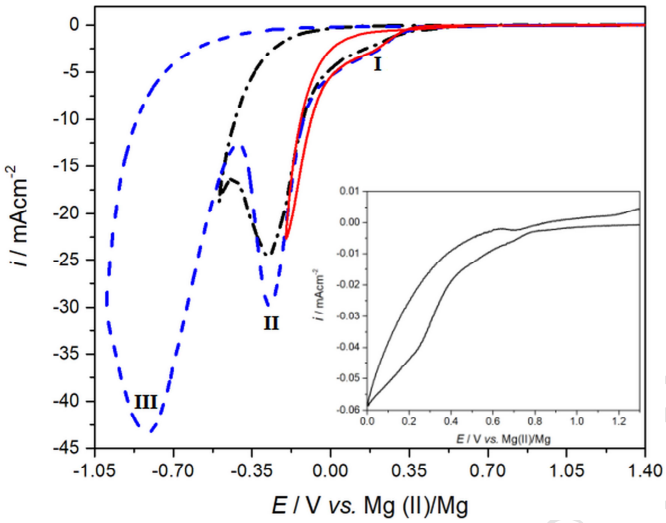

Fig. 1

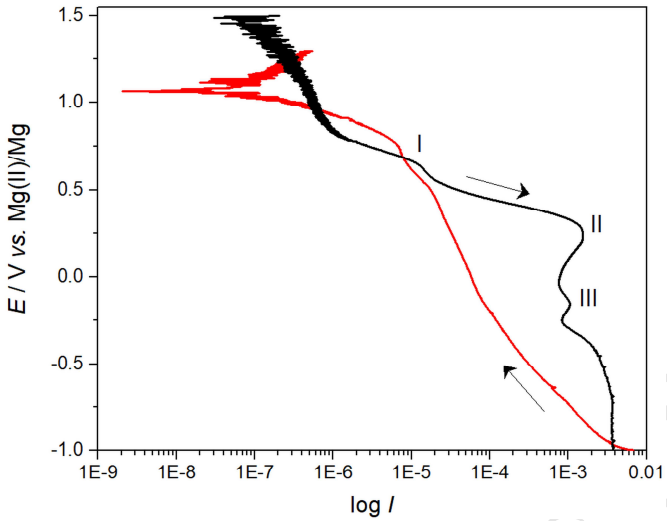

Fig. 2

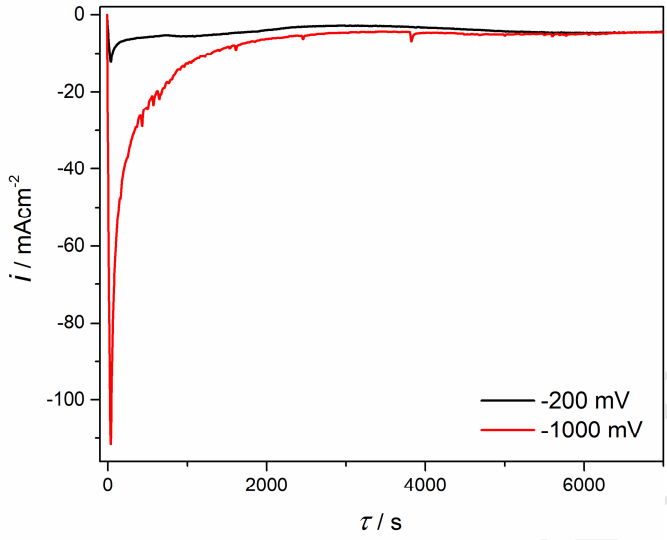

a)

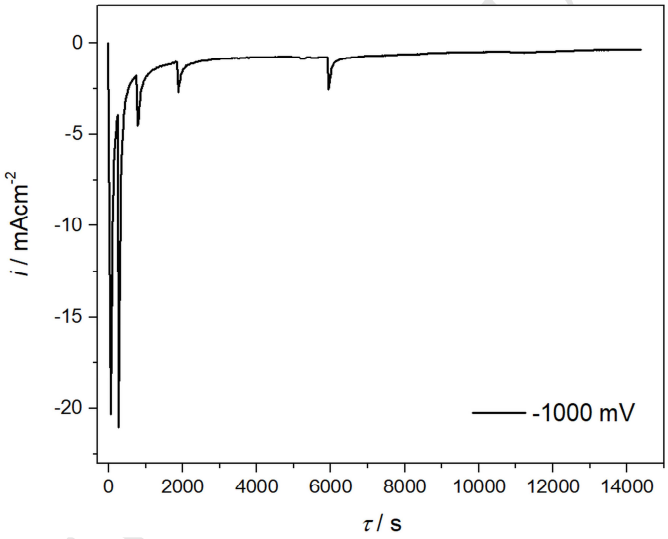

b)

Fig. 3

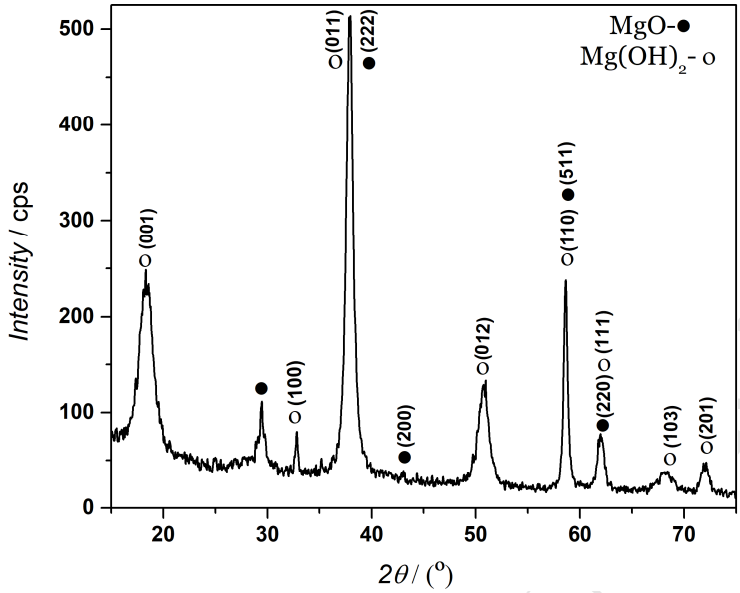

Fig. 4

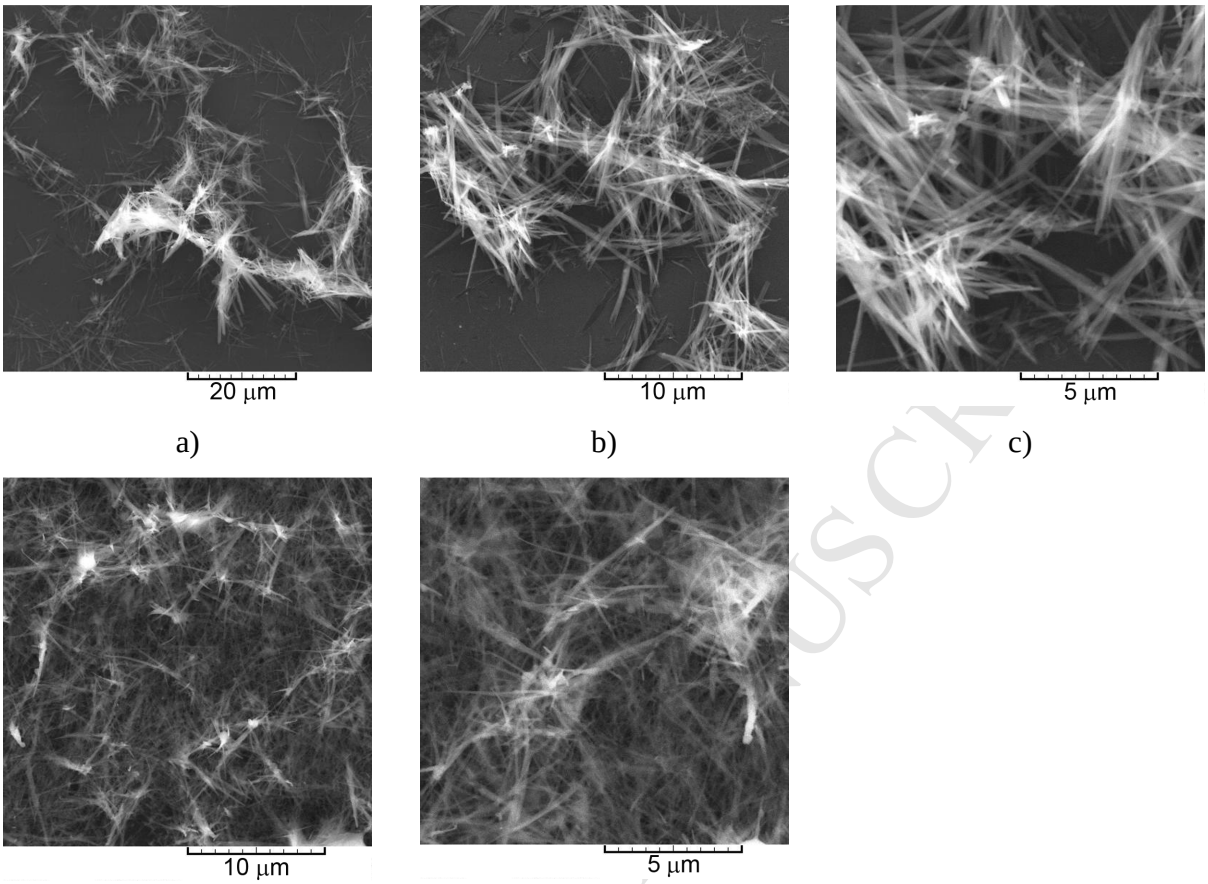

Fig. 5

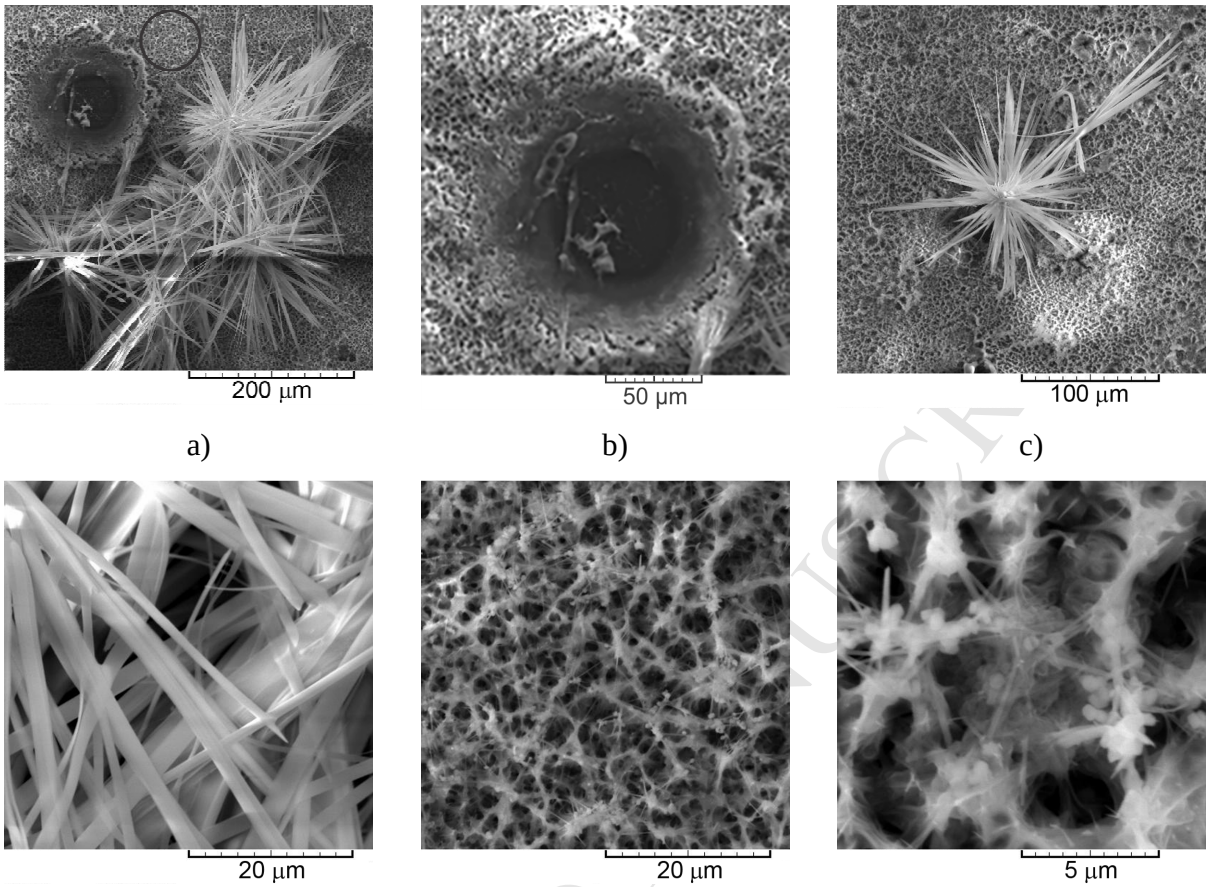

a) b) c)

d) e) f)

Fig. 6

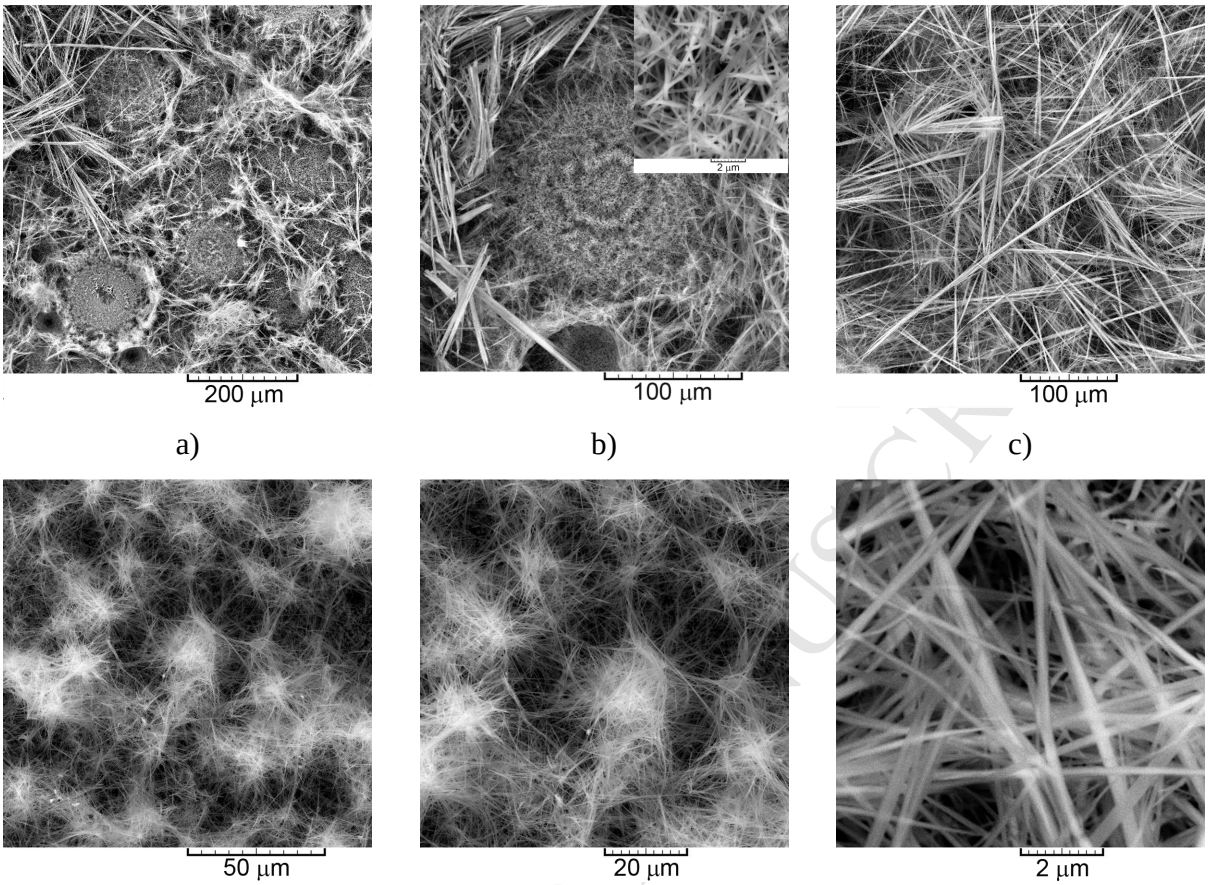

a) b) c)

d) e) f)

Fig. 7

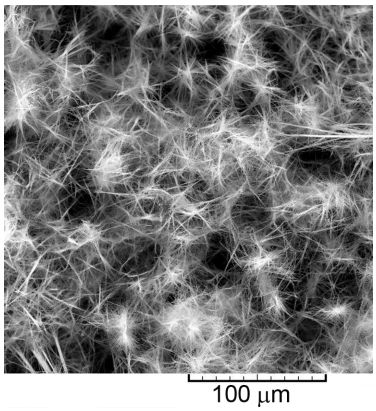

a)

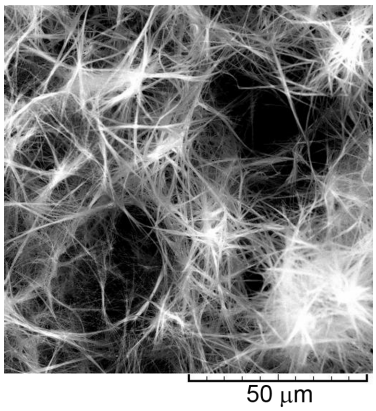

b)

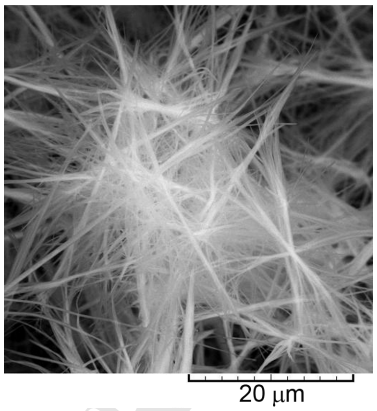

c)

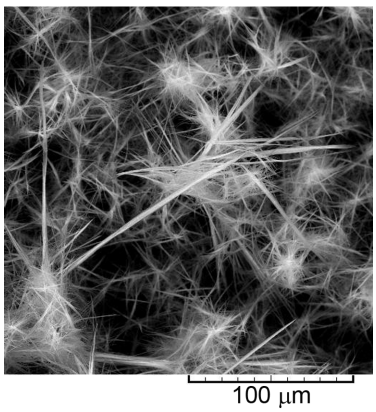

d)

Fig. 8

Research highlights

- Electrodeposition processes from magnesium nitrate melt were investigated.
- XRD analysis revealed formation of $MgO/Mg(OH)_2$ structures.
- Honeycomb-like and needle-like structures were formed by electrodeposition.
- It is possible to obtain MgO directly by electrodeposition from a nitrate melt.
- Chemistry of formation of $MgO/Mg(OH)_2$ structures was proposed.